Macromolecules

ARTICLE

pubs.acs.org/Macromolecules

Effects of Strong Confinement on the Glass-Transition Temperature in Simulated Atactic Polystyrene Films

Dmytro Hudzinskyy,*[,†,‡] Alexey V. Lyulin,[†] Arlette R. C. Baljon,[§] Nikolay K. Balabaev,[⊥] and Matthias A. J. Michels[†]

[†]Theory of Polymers and Soft Matter, Department of Applied Physics, Technische Universiteit Eindhoven, P.O. Box 513, 5600 MB Eindhoven, The Netherlands

[‡]Dutch Polymer Institute, P.O. Box 902, 5600 AX Eindhoven, The Netherlands

[§]Department of Physics, San Diego State University, San Diego, California 92182, United States

[⊥]Institute of Mathematical Problems of Biology, Pushchino 142290, Russia

ABSTRACT: We have performed molecular dynamics simulations to explore the influence of confinement on the glass-transition temperature T_g for supported atactic-polystyrene (aPS) thin films of different thickness (1−10 nm) and different strengths of attraction to the substrate (0.1−3.0 kcal/mol). The aPS films have been equilibrated in a melt at 540 K and further cooled down with a constant cooling velocity of 0.01 K/ps below T_g to room temperature, 300 K. On the basis of the density measurements, we have defined three different (substrate, middle, and surface) layers for each film. We found that the monomers close to the surface and in the substrate layer are partially oriented, which leads to more effective monomer packing. For the whole film the average density-based T_g value remains almost constant for films down to 2 nm thickness, where the middle layer vanishes. For the middle layer itself T_g does not depend on the total film thickness, while an increase up to 70 K is measured for the substrate layer depending on the strength of attraction to the actual substrate. The surface layer remains liquidlike in the whole temperature range (300−540 K). We claim that the redistribution of mass in the three film layers may explain the change with film thickness of the average T_g, if the latter is determined from linear fits of the average glass and melt densities.

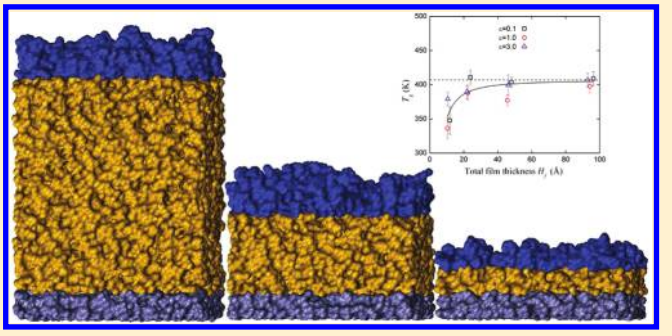

1. INTRODUCTION

With development of new experimental methods and powerful computers, huge attention is given to the physicochemical properties of polymers on the nanoscale and under strong confinement, as in thin films. With decreasing sizes of polymer films, it proves important to explore the influence of the confinement on the polymer glass-transition temperature T_g. In the literature it is shown that the presence of a supporting surface and a free interface may drastically change both the static and dynamic behavior of polymer chains in these films. Experimental studies have attempted to determine the T_g in films with different thicknesses,[1−28] using ellipsometry,[3−11] Brillouin light scattering,[10−12] X-ray reflectivity,[13−17] positron annihilation lifetime spectroscopy,[18] neutron reflectivity,[19,20] dielectric spectroscopy,[21−26] and calorimetric[27,28] methods.

Using ellipsometry, Keddie et al. have measured the temperature-dependent thickness of a polystyrene (PS) film supported by a hydrogen-passivated silicon surface up to ∼10 nm.[3] They found that the value of T_g deviates from that in bulk PS and decreases maximally ca. 25 K. This effect does not strongly depend on the PS molecular weight (PS M_w values were ranging in their study from 1.2×10^5 to 2.9×10^6, meaning that the PS samples are well entangled), but rather on the thickness of a film: the thinner the film, the larger the observed reduction of T_g. Lately Keddie reported that the reduction of T_g was also observed for poly(methyl methacrylate) (PMMA) films supported by different substrates, with different strengths of the polymer attraction to the substrate.[4] As substrates, either native oxide of silicon (strong attraction) or Au (weak attraction) was used. It was found that for weak attraction to the substrate the value of T_g for PMMA decreases by 10 K with the decrease of film thickness from ∼400 nm down to ∼40 nm, while for strong attraction the T_g value slightly increases. A similar conclusion has been made by Fryer using thermal analysis and ellipsometry for PS and PMMA supported by polar (SiO_x, strong attraction for PMMA) and nonpolar (SiO_x-hexamethyldisilizane (HMDS), weak attraction for PMMA) substrates.[29] Note that for PS the attractions to these two substrates are the same and that no dependence of T_g on the nature of the substrate has been found. For PS the T_g decreases by ∼25 K for both substrates, but for

Received: November 11, 2010
Revised: February 10, 2011
Published: March 09, 2011

PMMA the T_g decreases by ~10 K for the nonpolar substrate and increases by ~7 K for the polar substrate.

The reduction of T_g for ultrathin (6−489 nm) aPS films supported by an Al-deposited slide glass was also observed by Fukao et al.,[21] using dielectric measurements, with four different aPS molecular weights, ranging from $M_w = 3.6 \times 10^3$ to $M_w = 1.8 \times 10^6$ (i.e., below and above the entanglement molecular weight for aPS $M_e = 1.3 \times 10^4$).[21] These results are comparable with the recent observations of Lupaşcu et al., who studied PS with capacitive dilatometry (CD).[26] However, it is interesting to note that in the early publication of Lupaşcu the T_g value measured using the same method slightly increases with decreasing film thickness.[25] This completely different film-thickness behavior of T_g may be explained by some differences in experimental conditions. For example, the differences in the annealing protocol, 12 h in both cases but at different temperatures, $T = 373$ K and $T = 393$ K,[25,26] can be important. However, no thickness dependence of T_g was observed by Lupaşcu and others when ac-calorimetry (AC) was used instead.[25] No changes in the position of T_g have been detected either by Efremov et al.,[27,28] or more recently by Serghei et al.,[24] for supported PS and PMMA films down to ~3 and ~8 nm, using ultrasensitive differential scanning calorimetry and dielectric spectroscopy together with ac-calorimetry, respectively.

In addition to the extensive studies of supported films many experiments with free-standing films of the same or comparable thickness have been made, which show an even larger reduction of T_g. The first measurements of T_g values in free-standing PS films have been done by Forrest et al. using Brillouin light scattering for films of 29−70 nm.[12] It was found that the glass-transition temperature decreases linearly with film thickness, maximally ca. 70 K for the thinnest films as compared to the bulk.

We have already mentioned the possible effects of annealing on T_g reduction in thin films.[25,26] Kanaya et al. have performed neutron-reflectivity measurements on thin PS films supported by a silicon substrate to see the effect of annealing on the thickness and T_g of the films.[20] They considered two films that were annealed in vacuum both above and below T_g, with the same annealing time for both samples. The films were named strongly and weakly annealed, respectively. It was shown that T_g decreases with decreasing film thickness and that the value of T_g is almost independent of thermal history, i.e., whether it is strongly or weakly annealed. Experiments about the influence of annealing time on T_g have also been performed by Efremov for films from 400 nm down to 3 nm.[28] The measurements of T_g were made for series of samples with different thermal history, and no appreciable dependence of T_g on film thickness was found.

So the available experimental data still cannot produce a clear picture of the variation of T_g in thin polymer films, neither can they suggest a physical mechanism for such a phenomenon. The effects of the substrate, free interface, and specific polymer−substrate interactions are very difficult to separate in experimental practice, and therefore their individual influences cannot be fully recognized either. Such a separation can, in principle, be carried out in a dynamic computer simulation. The existing computer simulations for model polymers report significant deviations of T_g from the bulk values if the macromolecules are spatially confined.[30−35] However, it should be noticed that the most common experimental techniques to measure the T_g of thin polymer films are those that probe the thermal expansion of the sample (ellipsometry) or those that study the slowing down of polymer segmental dynamics (dielectric spectroscopy, for example) that is connected to the significant increase of the viscosity of the system. Both the temperature dependence of the film thickness and the temperature dependence of the segmental dynamics strongly depend on the cooling rate, which in experiment is orders of magnitude slower than in any molecular dynamics simulation. As a consequence, T_g is also strongly cooling rate dependent and is in computer simulations always shifted to larger values. Baschnagel et al. have used two temperatures to characterize the glass transition: the Vogel−Fulcher−Tammann (VFT) temperature, T_0, and the critical temperature T_c of the mode-coupling theory (MCT).[32,36] The simulated T_g is not equal to either of them but lays somewhere in between, $T_0 \leq T_g \leq T_c$. A decrease of T_0 and T_c for smaller film thicknesses has been observed in these simulations, and it has been suggested that hence the T_g value should decrease for stronger confinements.

Computer simulations of freely standing atactic-polypropylene films at a fixed temperature well below their experimental T_g have been performed by Mansfield and Theodorou.[37] Their results suggest that the role of a free interface is to increase the segmental mobility there and, as a consequence, to reduce the average T_g value for the whole film. The free interface behaves as a melt (i.e., it has a lower T_g) in contrast to the frozen glassy middle (bulklike) layer of the film.

As mentioned before, the value of T_g also depends on the type of polymer−substrate interaction. Because of the presence of specific interactions between a substrate and a polymer chain some ordering of chain segments or monomers is induced near the substrate. An attempt to measure this ordering has been made in experimental studies as well as computer simulations.[37−42] Using an oblique-polarized-ray method, Grishchenko et al. have recently found that the segmental orientational order parameter decreases with increasing distance from the polymer−air interface.[41] The observed ordering effects have not been connected to deviations of the film T_g value from that of the bulk.

In the studies discussed above the glass-transition temperature of the polymer film has been measured as an average property, meaning that the very different (both from the point of view of monomer packing and dynamics) internal film regions, with different densities and segmental mobilities (and, probably, different values of the corresponding local T_g) are taken into account in an average way. The explanation of the T_g deviation from the bulk value could be contained in a two- or three-layer model,[18,21] where the presence of two (in free-standing films) or three (in supported films) kinds of internal layers are considered. According to this model, a thin polymer film on a substrate consists of a dead layer,[18] which is in a contact with the substrate (and which is of course absent in a free-standing film) and has almost no segmental mobility, a bulklike layer, which has the same mobility as a bulk polymer, and a surface layer, which has a higher mobility. This difference in the mobility may lead to different values of T_g: the T_g for a substrate layer, with almost immobile polymer segments, can be higher than the T_g value for a bulklike middle layer, while for a surface layer, with enhanced mobility, it can be lower.

The first experimental measurements of T_g in different layers of PS films were made by Bliznyuk et al. (supported films) and Ellison and Torkelson (both free-standing and supported films), using scanning force microscopy and a fluorescence/multilayer method, respectively.[43,44] Bliznyuk et al. show that for films down to ~25 nm and PS chains of $M_n = 116$ kg/mol the glass-transition temperature in the surface region decreases by ~33 K with

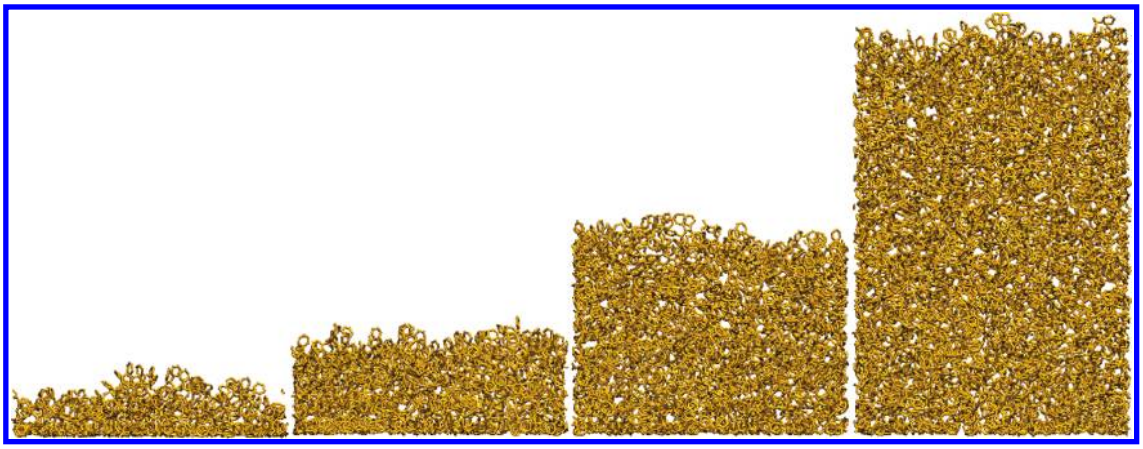

Figure 1. Typical snapshots of the supported thin aPS films of increasing thickness (from 4 chains (left) to 32 chains (right), thickness about 1.5, 2.5, 5, and 9.5 nm, respectively) at T = 540 K.

decreasing film thickness.[43] Ellison and Torkelson have found that when the thicknesses of all three layers are comparable (~12 nm), T_g decreases by 14, 5, and 4 K for surface, middle, and substrate layers, respectively.[44] These observations (a decrease of T_g values in all separate film layers) obviously cannot be used to explain a possible increase of the average value of T_g as, for example, suggested by the three-layer model. Recently, Mukhopadnayay et al. reported that structural changes in PS (e.g., density variations) occur for film thicknesses $H \leq 4R_g$, with R_g the radius of gyration. An increase in excluded volume that is connected with these changes has been used to explain the reduction of T_g in PS films thinner than $4R_g$.[45]

The aim of the present study is to perform molecular dynamics (MD) simulations of the glass-transition temperature of supported atactic polystyrene (aPS) films, both averaged over each film and in different layers of these films. The main purpose is to study the possible variation with film thickness of the average T_g as well as the variation of T_g in three different layers: substrate, middle, and surface. The simulations have been performed for films of four different thicknesses, spanning a factor 8, and for three different strengths of the attraction to the substrate, spanning a factor 30.

The paper is organized as follows. In section 2 we give the description of the model of the supported aPS film together with the description of the whole simulation procedure. In section 3 we discuss the conformational features of aPS chains in thin supported films, including the ordering of chain monomers. In that section we also present the simulation results for T_g, for both the whole film and the separate layers. These results are based on determination of the film or layer thickness vs temperature, similar to what is done experimentally with ellipsometry, and on the calculated densities vs temperature. In the Discussion section we analyze the possible trends in T_g behavior for the separate layers and try to rationalize our findings. Our conclusions are given in the last section of the paper.

2. MODEL AND SIMULATION DETAILS

2.1. Model and Algorithm. The chosen model is the same as the united-atom model used in our recent paper.[46] In a united-atom representation of aPS there are no explicit hydrogen atoms present, but instead, they are collapsed onto the carbon atoms and the combined atoms are treated as effective particles. The motivation of using this model for aPS is that computations are much faster for the united-atom model than for the all-atom model.[47]

We have performed simulations for supported aPS films of different thickness. Each film consists of 4, 8, 16, or 32 chains, with 80 monomers per chain (molecular weight $M_w = 8.4 \times 10^3$, below the entanglement molecular weight of $M_w = 1.3 \times 10^4$), and 2564, 5128, 10 256, 20 512 united atoms, respectively. The average gyration radius of these chains is found to be about 2.0 nm. Periodic boundary conditions are implemented in the x and y directions only (the box size is fixed to 7.0 nm × 7.0 nm). The four aPS films of different thickness are shown in Figure 1.

The monomer unit consists of two backbone (−CH−CH_2−) atoms and the phenyl ring—the aromatic side group attached to the backbone. The stereochemic configurations of the aromatic groups were generated at random so that the ratio of the number of *meso* to the number of *racemic* dyads was near unity.

All the interactions between aPS united atoms are given by the following potential:

$$U_{PS} = \sum_{i,j} \varepsilon_{ij} \left[\left(\frac{\sigma_{ij}}{r_{ij}} \right)^{12} - 2 \left(\frac{\sigma_{ij}}{r_{ij}} \right)^{6} \right] + \sum_{i,j} k_{l,ij} (r_{ij} - l_{ij})^2 + \sum_{i,j,k} k_{\theta,ijk} (\theta_{ijk} - \theta_{0,ijk})^2 + \sum_{i,j,k,l} k_{\phi,ijkl} \cos(n\phi_{ijkl}) \quad (1)$$

The potential U_{PS} includes the following contributions: nonbonded interactions (~ε_{ij}) between united atoms that are on different chains or are separated by more than three covalent bonds ($\varepsilon_{ij} \sim 0.1$ kcal/mol); a stretching potential (~k_l) between two neighboring atoms i and j sharing their valence electrons; a bending potential (~k_θ) for all bond angles, including those in the phenyl rings; proper-torsion and improper-torsion potentials (~k_ϕ). Coulomb interactions are not taken into account. For more details of the potential contributions and the values of all the potential constants, we refer to ref 48.

In order to simulate supported aPS films, a completely smooth, structureless substrate is introduced at $z = 0$ in the xy-plane of the simulation box. To simulate the monomer−substrate interactions, a truncated 9−3 Lennard-Jones (LJ) potential is chosen:

$$U_{sub}(z) = \begin{cases} U_{sub}(z) - U_{sub}(z_{cut}), & z < z_{cut} \\ 0, & z > z_{cut} \end{cases}$$

$$U_{sub}(z) = \frac{1}{2} \varepsilon \left\{ \left(\frac{z_{min}}{z} \right)^9 - 3 \left(\frac{z_{min}}{z} \right)^3 \right\} \quad (2)$$

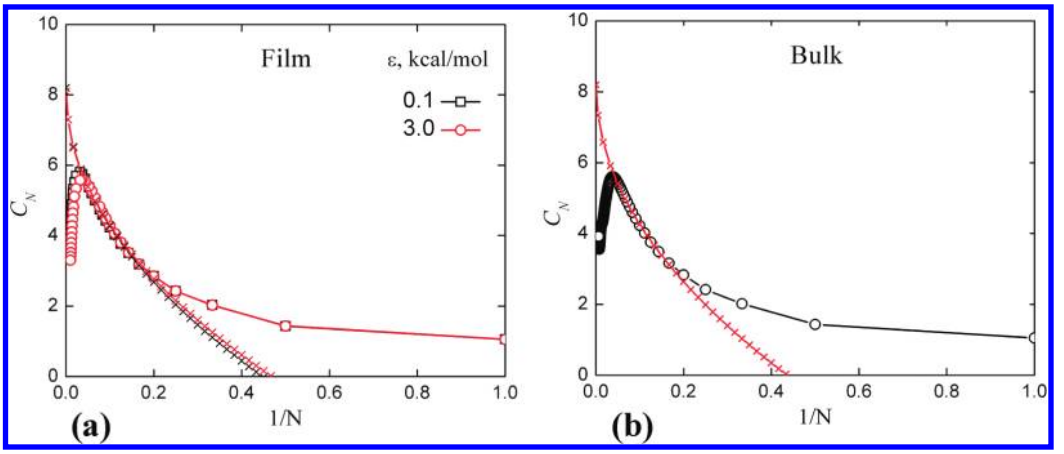

Figure 2. Characteristic ratio C_N at $T = 300$ K as a function of the inverse of the number of backbone bonds for aPS in (a) thin supported film with eight chains and different strengths of attraction to the substrate and (b) in a bulk polymer.[56] The open symbols (squares and circles) connected by lines correspond to the MD simulations results, and connected crosses are fits with eq 4.

Here, z denotes the distance from the monomer to the substrate and ε is the strength of the attraction to the substrate. $z_{min} = 0.3$ nm is the distance at the minimum of the potential, and $z_{cut} = 0.9$ nm is the cutoff distance. This potential is similar to that used by Müller et al. in simulations for a bead−spring model film, except that in their case the potential was not truncated or shifted.[49] For a bead−spring model the wetting transition occurs at $\varepsilon = 0.4$ kcal/mol at $T = 300$ K,[49] while in the present MD simulations the potential strength ε varies from 0.1 kcal/mol (nonwetting) to 3.0 kcal/mol (complete wetting). This potential mimics the van der Waals interactions between the atoms of the substrate and polymer segments and can be obtained by integrating the 12−6 LJ potential over a half space.[50]

The leapfrog variant of the velocity Verlet algorithm has been used to integrate Newton's equations of motion with an integration time step $\Delta t = 4$ fs.[51] The equilibration has been performed in NVT and NPT ensembles with the help of the collisional thermostat and Berendsen barostat.[51,52]

2.2. Equilibration and Annealing. At the beginning of the simulations all aPS chains for each film were stretched along the z-axis and were located inside a large simulation box (polymer "gas phase") of typically $(20-40)^3$ nm^3 to avoid possible close contacts of nonbonded atoms. The box was allowed to relax for a sufficiently long time (10−20 ns, depending on the size of the modeled film), under a fixed external pressure (1−700 MPa). Each film is equilibrated at an initial high temperature of $T = 540$ K in a high-mobility melt state. The first half of the equilibration process has been performed with a purely repulsive substrate in order to avoid immediate adsorption of the chain ends to the substrate. In a later stage the full 9−3 LJ potential, eq 2, has been used. For each film the last 5 ns of the trajectory have been used to calculate the density profile and the film thickness at the fixed initial temperature ($T = 540$ K). The quality of the equilibration was controlled by measuring various statistical properties, such as the individual-chain radius of gyration, the chain end-to-end distance, and the characteristic ratio for different intermediate distances within each aPS chain. The equilibration has also been checked by performing additional simulations for 16 independent samples of the 8-chain aPS film with $\varepsilon = 1.0$ kcal/mol, equilibrated initially at $T = 540$ K. These samples were further heated up to $T = 600$ K, and an additional equilibration was performed for 10 ns at this temperature. For these samples we calculated the same statistical properties that are listed above and found no difference in their conformational properties at two different temperatures. For all films, depending on their size, the external pressure at $T = 540$ K was adjusted in order to reach a density in the middle of the film as close as possible to the experimental bulk density of 0.914 g/cm^3.[53] Finding the correct pressure for each separate case proved computationally demanding. As a result, the densities in the middle of the simulated films at $T = 540$ K approach the experimental bulk value with a deviation of at most 2%. For the purpose of the Discussion section we have performed additional simulations of a 32-chain film with a strong attraction to the substrate and at different external pressures. In this case the experimental density in the middle of the film was reproduced well within 1%.

The pressure correction was kept constant for each film at all simulated temperatures, implying that any density deviation would probably be nearly constant across the temperature range; however, the pressure correction was different for films of different thicknesses and different strengths of adsorption.

After the equilibration was finished continuous cooling was performed with a constant cooling velocity of 0.01 K/ps down to room temperature, $T = 300$ K. Our previous studies show that such a cooling rate corresponds to computationally well-aged united-atom polymer samples.[54] During the cooling process the trajectories have been saved every 20 K for a further analysis. Moreover, for each intermediate temperature 1 ns MD production runs in NPT ensemble have been performed as well. In order to increase statistics, the simulations have been done for four independent samples for each film of the specific composition and specific strength of attraction to the substrate.

3. RESULTS

3.1. Characteristic Ratio. In order to verify the quality of the equilibration of the simulated aPS films, the characteristic ratio

$$C_N = \left\langle \frac{R^2(N)}{N l_b^2} \right\rangle \tag{3}$$

has been calculated first, where $R^2(N)$ is the squared distance between two segments separated by N backbone bonds and l_b is the equilibrium length of the chemical bond in the aPS backbone, $l_b = 0.153$ nm.[55]

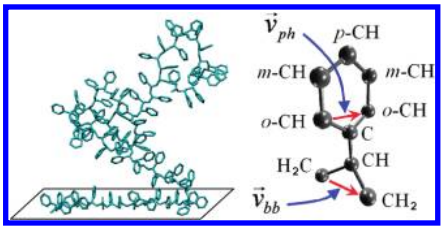

Figure 3. Left: typical snapshot of one aPS chain in a many-chain supported film close to the substrate at $T = 540$ K and $\varepsilon = 3.0$ kcal/mol. Right: the aPS monomer with the naming convention of the united atoms, shown together with two vectors, $\vec{v}_{ph}$ for the phenyl ring and $\vec{v}_{bb}$ for the backbone orientation, that are chosen to measure the order parameter P_2. Here o = ortho, m = meta, and p = para.

The simulation results for the characteristic ratio at room temperature in thin supported films and in a bulk sample are shown in Figure 2. The results for the bulk simulations are taken from our previous studies.[55] The values of C_∞ have been calculated by fitting C_N vs $1/N$ as suggested in[57,59]

$$C_N = C_\infty(1 - \alpha N^{-1/2}) \quad (4)$$

Note that the long-chain limit (C_∞) proves independent of the strength of attraction to the substrate; $C_\infty = 8.2 \pm 0.1$ for a weak attraction ($\varepsilon = 0.1$ kcal/mol), and $C_\infty = 8.1 \pm 0.3$ for a strong attraction ($\varepsilon = 3.0$ kcal/mol). These results are hardly influenced by the confinement effects: for bulk aPS at $T = 300$ K we earlier produced the value of $C_\infty = 8.3 \pm 0.1$.[58]

For both weak and strong attractions the fitting parameter α in eq 4 is very close to 1.5. Comparing with the parameter α obtained analytically in eq 16 of ref 59, we note that in ref 59 the number of Kuhn segments was used instead of number of chemical bonds in eq 4. To match the simulations with the notation of ref 59, we recalculate the value of α in eq 4 using Kuhn segments and introducing new prefactor α^*. We found that the analytically calculated value of α^* is equal to 0.48, while in the present simulations $\alpha^* = 0.43$. The small difference is probably connected to rather moderate chain length in the present simulations.

To check the equilibration, we have also performed additional simulations of the 8-chain aPS film for the wetting case ($\varepsilon = 1.0$ kcal/mol), equilibrated subsequently at two different temperatures, $T = 540$ K and $T = 600$ K, as explained above. We found, as for the values of C_∞, that within statistical error the temperature dependences of the melt density are the same for both films; in the glassy region some deviation occurs.

3.2. Monomer Orientation and Ordering. To measure the possible local ordering of monomers in the supported polymer films, the segmental orientation of chains has been calculated. To do so, we defined two vectors, $\vec{v}_{ph}$, which connects two united atoms, o-CH−o-CH, inside the phenyl side group, and $\vec{v}_{bb}$, directed along the backbone (H_2C-CH_2), for all monomers in a film, as shown in Figure 3. The order in the orientations of different segments is then expressed for each vector in terms of the second-rank tensor:

$$\langle S_{\alpha\beta}\rangle = \frac{1}{N_{mon}}\left(\frac{3}{2}\sum_{k=1}^{N_{mon}}(\hat{X}_\alpha^k \cdot \hat{X}_\beta^k) - \frac{1}{2}\delta_{\alpha\beta}\right) \quad (\alpha,\beta = x,y,z) \quad (5)$$

where $\hat{X}_{\alpha,\beta} = \vec{v}_{ph(bb),\alpha(\beta)}/|\vec{v}_{ph(bb),\alpha(\beta)}|$; the summation is made over all monomers, and $\delta_{\alpha\beta}$ is the Kronecker delta. Angular brackets $\langle ... \rangle$ denote an average over all segments as well as a time average. $S_{\alpha\beta}$ is a real symmetric matrix and can be diagonalized to find the eigenvalues and eigenvectors.

The order parameter P_2 was defined as the ensemble average of the largest eigenvalue of the diagonalized order tensor $\tilde{S}_{\alpha\beta}$. The average direction of alignment is defined by its corresponding eigenvector. In Figure 4, the order parameter P_2 for the backbone vector $\vec{v}_{bb}$ (a) and for the phenyl-ring vector $\vec{v}_{ph}$ (b) is calculated inside subsequent layers of 0.35 nm thickness.

We found that the order parameter of both the backbone and the phenyl vector is rather small, $P_2 \sim 0.1$, except for thin regions close to the substrate and free interface.

Close to the substrate and free interface, the order parameter of the backbone vectors (Figure 4a) is in the range of $P_2 \sim 0.21-0.24$ for both the nonwetting and strong-wetting substrates. For the phenyl vectors close to the free interface we observe slight increase of P_2 both for nonwetting and strong-wetting substrates while close to the substrate highly oriented phenyl vectors for the strong-wetting substrate are observed (Figure 4b). This region of enhanced ordering spans about ~1 nm. Analyzing the eigenvectors we found that at both sides the backbone vectors (H_2C-CH_2, see Figure 3) are oriented in a plane parallel to the interface while the phenyl-ring vectors (o-CH−o-CH, see Figure 3) are preferably oriented along the normal to both the plane of the free surface and plane of the substrate. These results at least qualitatively support the experimental findings of Grishchenko et al., who found that the order parameter decreases exponentially with the distance from the interface boundary.[41] They also found that the PS chain segments are oriented mainly parallel to the surface of a film, in agreement with the present simulations.

3.3. Density Profiles. The density profiles at $T = 540$ K of the supported thin aPS films with different thicknesses and different strengths of the attraction to the substrate are shown in Figure 6. The overall shape of the density profile for supported films is qualitatively different from that for free-standing films and quite similar to that observed in previous simulations for model supported polymer films.[31,60,61] For a free-standing film the density profile has an almost symmetric shape, since the film has two identical free surfaces. For a supported film the density profile has a nonsymmetric shape, since one side of the film is confined by a substrate.

By considering the density profile for supported films, we are able to recognize three stratified regions (see Figure 5, left panel) with different density behavior. These layered regions are the region near the polymer/substrate interface (*substrate* layer) with sharp density variations, the plateau (*middle* layer) with almost constant density, and the polymer/vacuum interface (*surface* layer) with a monotonically decreasing density.

The density profile for a 4-chain film is not depicted in Figure 5 and is the exception, since this film is so thin that the *middle* layer does not exist. At rather high temperatures the density in the middle of a film is almost constant (at $T = 540$ K its value has been fitted to the bulk value) and does not depend on the strength of attraction to the substrate. As can be also seen from the figure, the substrate only weakly influences the thickness of a film. The difference in film thickness for a weak ($\varepsilon = 0.1$ kcal/mol) and a strong ($\varepsilon = 1.0$, 3.0 kcal/mol) attraction to the substrate is for all simulated films about 0.3 nm.

The density profile near the polymer/substrate interface is enlarged in the inset of Figure 5 (left panel). With increasing strength of attraction the density near the substrate increases and

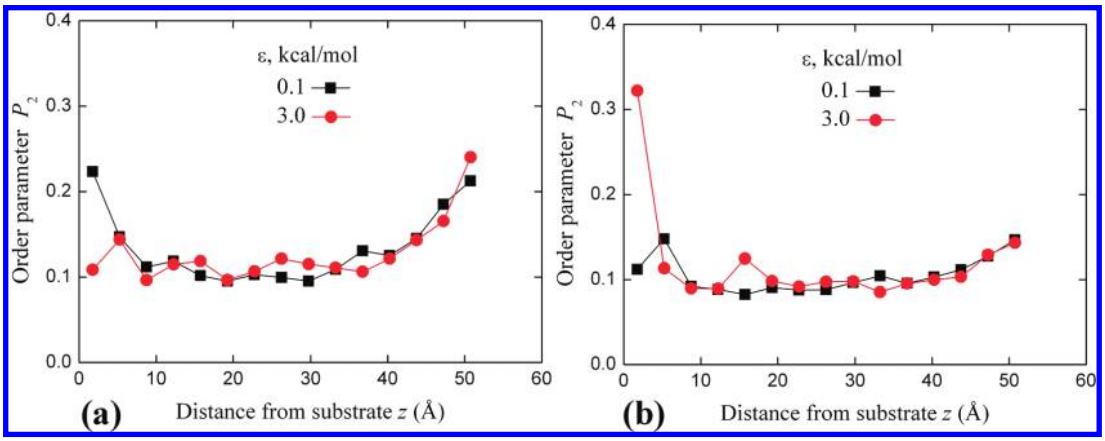

Figure 4. Order parameter P_2 for the aPS backbone vector $\vec{v}_{bb}$ (a), and for the phenyl-ring vector $\vec{v}_{ph}$ (b), for a 16-chains film at T = 540 K and for different strengths of the attraction to the substrate.

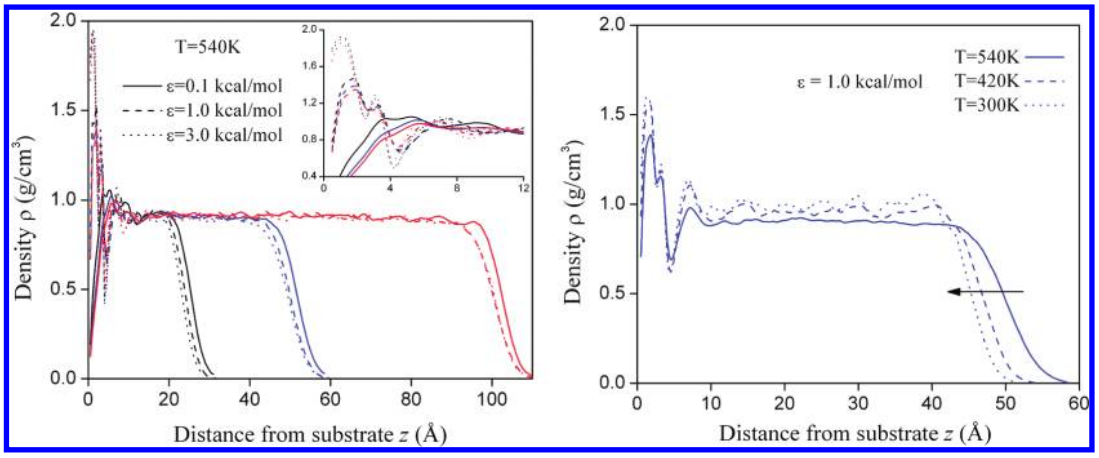

Figure 5. Left: density profiles at T = 540 K for supported thin aPS films of 8, 16, and 32 chains with different strengths of attraction to the substrate. The solid lines correspond to weak (ε = 0.1 kcal/mol) attraction while the dashed and dotted lines correspond to strong (ε = 1.0 and 3.0 kcal/mol) attraction to the substrate. Right: density profiles for the film of 16 chains with strong attraction to the substrate at three different temperatures. The arrow indicates the direction of the temperature decrease.

starts to fluctuate. For a strong attraction the shape of the density profile is almost identical for all simulated films. We also checked the influence of the cutoff radius z_{cut} of the attractive substrate, by decreasing it to 0.45 nm and by increasing it to 1.8 nm. These changes do not noticeably influence the density profile, meaning that the stratified pattern in a first approximation does not depend on this cutoff distance z_{cut}.

In Figure 5 (right panel) it is also shown how the density profile (16-chain film, ε = 1.0 kcal/mol) changes with decreasing temperature, from T = 540 K to T = 300 K. We observe that the thickness of the film decreases, leading to a density increase both in the middle of the film and in the substrate layer. In the middle of the film the density increases uniformly while close to the substrate the density fluctuations are strongly enhanced. These fluctuations probably reflect the ordering of the monomers and their more close packing near the wetted substrate.

3.4. Glass Transition Temperature. To calculate the glass-transition temperatures in different film regions, we must define the three different film layers quantitatively (see Figure 6). To start with, we define in the density profile two peaks in the middle layer (two vertical arrows in Figure 6). One peak is chosen as the first maximum that appears after the monotonic increase of the

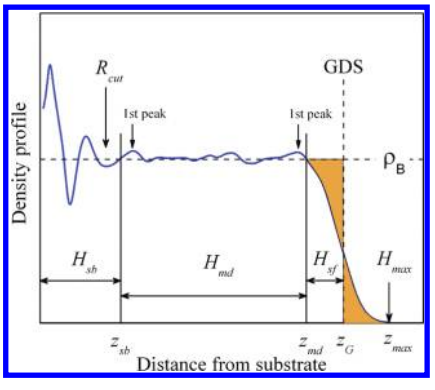

Figure 6. Density profile for a supported aPS film with 16 chains at T = 540 K and the definition of three layers with different density behavior: substrate (*sb*), middle (*md*), and surface (*sf*) (see the explanation in the text).

density from the free interface toward the middle of the film. The other peak is chosen as the first one that appears after the cutting distance z_{cut} from the substrate. In practice, there is only one maximum after that distance, so it is the only reasonable choice.

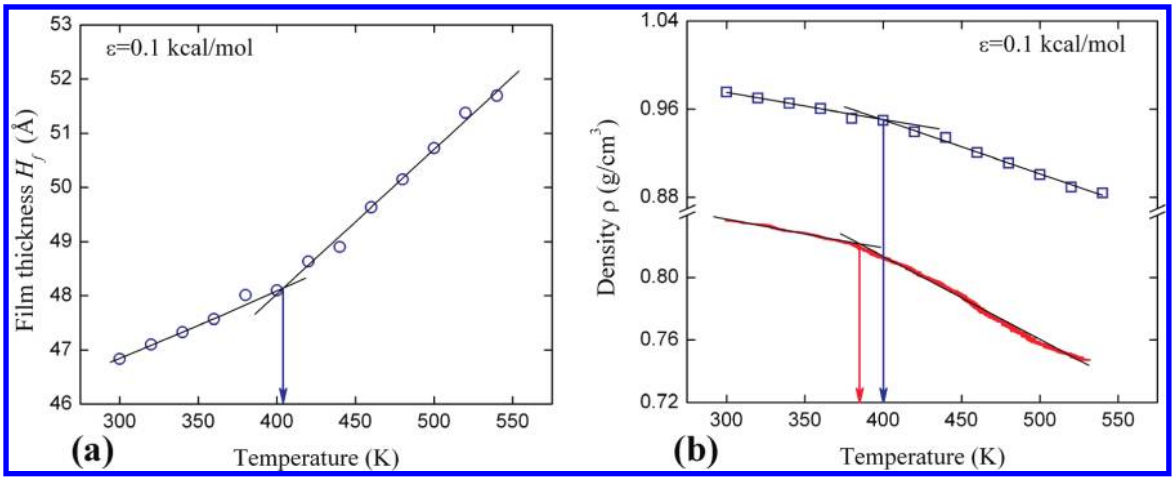

Figure 7. Film thickness (a) and average film density (b) as a function of temperature for aPS film with 16 chains in the case of a weak attraction ($\varepsilon = 0.1$ kcal/mol) to the substrate. The circles represent the thickness H_f of the whole film using the GDS. The squares represent the average density over the whole film, where the thickness of the film is measured as the distance from the substrate to the GDS. The red solid line represents the average density over the whole film, where the thickness of a film is calculated as the distance from the substrate to the maximal value H_{max} of all z coordinates.

Table 1. Slopes $-(d\rho/dT)_{melt,glass}$ for Simulated Thin aPS Films and Their Substrate and Middle Layers[a]

	nonwetting		wetting	
$\times 10^{-4}$ [g cm^{-3} K^{-1}]	$(d\rho/dT)_{melt}$	$(d\rho/dT)_{glass}$	$(d\rho/dT)_{melt}$	$(d\rho/dT)_{glass}$
whole film	4.7 ± 0.2	2.3 ± 0.2	4.5 ± 0.3	2.1 ± 0.2
middle	4.8 ± 0.3	2.5 ± 0.4	4.8 ± 0.6	2.4 ± 0.4
substrate	5.4 ± 0.8	1.9 ± 0.5	4.3 ± 0.7	1.7 ± 0.2

[a] Data are averaged over films with 8, 16, and 32 chains; in the wetting case data are also averaged over substrate attraction strengths $\varepsilon = 1.0$ and 3.0 kcal/mol.

Table 2. Expansion Coefficients α and Glass-Transition Points (T_g, ρ_g) for Simulated aPS Films and for Bulk aPS[a]

	whole film (nonwetting)	whole film (wetting)	bulk (exp)[b]	bulk (simul)[c]
α_{melt},[d] 10^{-4} [K^{-1}]	5.3 ± 0.3	4.8 ± 0.4	6.8 ± 0.1	5.7 ± 0.1
α_{glass},[d] 10^{-4} [K^{-1}]	2.4 ± 0.2	2.0 ± 0.2	2.2 ± 0.2	2.3 ± 0.1
T_g [K]	393 ± 30	384 ± 22	363 ± 2	380 ± 10
ρ_g [g/cm^3]	0.95	1.00	1.02	1.00

[a] Data are averaged over films with 8, 16, and 32 chains; in the wetting case data are also averaged over substrate attraction strengths $\varepsilon = 1.0$ and 3.0 kcal/mol. [b] Data are calculated from ref 53. [c] Data are calculated from ref 62. [d] The thermal expansion coefficients in the melt and glassy states are calculated at $T = 540$ K and $T = 300$ K, respectively.

Then the average density (horizontal dashed line in Figure 6) between these two peaks has been calculated. As mentioned before, the external pressure was at $T = 540$ K adjusted to obtain this average density in the middle layer as close to the PS bulk density as possible.

Points of intersection of the horizontal dashed line with the density profile near the peak positions, z_{sb} and z_{md}, are used to define the middle layer; the thickness of the polymer/substrate interphase and the thickness of the middle layer follow as $H_{sb} = z_{sb}$ and $H_{md} = z_{md} - z_{sb}$, respectively. To define the thickness H_{sf} of the free surface and the thickness of the whole film ($H_f = H_{sb} + H_{md} + H_{sf}$) as well, we construct the Gibbs dividing surface (GDS) which is depicted at $z_G = z_{sf}$ by a vertical dashed line; it has been defined such that the areas of the colored regions in Figure 6 taken with different signs sum to zero. Then $H_{sf} = z_{sf} - z_{md}$. We also define H_{max} as the maximal value of the z coordinate for the PS united atoms in a film. To derive T_g, two numerical methods have been followed. First the thickness H_f of the whole film has been measured during the cooling process (Figure 7a). Second, the temperature variation of the average film density has been measured; the latter has been calculated in two different ways (Figure 7b).

The first way is to calculate the average density (red line, Figure 7b) as the total mass divided by the film volume $V = L_x \times L_y \times L_z$ with $L_x = L_y = 7$ nm and $L_z = H_{max}$. This quantity is directly computed during the cooling process. The second way (squares, Figure 7b) is similar except that the film thickness is taken using the GDS, so $L_z = H_f$. In both cases the glass-transition temperature is measured by selecting two linear regions of the data corresponding to high and low temperatures, fitting them by straight lines, and finding the intersection point (Figure 7) (note that this eliminates any constant density deviation as discussed above). We should also note here that the determination of T_g from the double-tangent construction is subject to statistical errors, and the value of T_g could depend on the length of the chosen interval. Nevertheless, our calculations show that the average values of the glass-transition temperature calculated using data intervals of different length coincide within error bars.

The average-density method with the thickness of a film calculated as the distance from the substrate to the maximal value H_{max} of the z coordinates is not used for further analysis; in this case we have not found any thickness dependence of T_g because of rather large fluctuations of the results. The accuracy is decreased here in particular because much fluctuating empty space is taken into account when calculating a film volume. The method based on the film density defined with the help of the GDS gives essentially the same results as that based directly on the film thickness H_f.

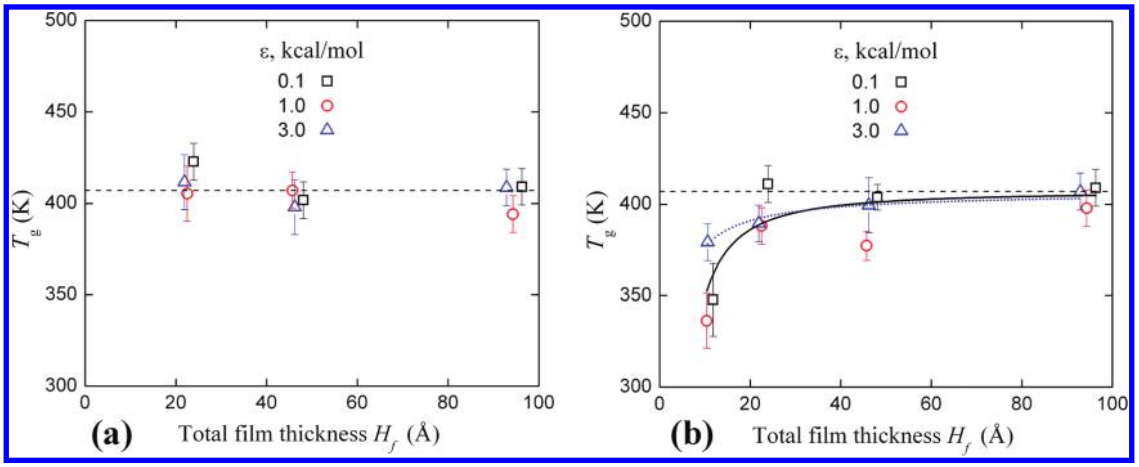

Figure 8. Thickness dependence of T_g of the middle layer (a) and of the whole film (b) for the case of weak (ε = 0.1 kcal/mol) and strong (ε = 1.0, 3.0 kcal/mol) attraction to the substrate. The dashed lines represent the average T_g value for the middle layer. The solid and dotted lines denote the best fit of all data points and of the data for strong (ε = 3.0 kcal/mol) attraction to the substrate, respectively, using eq 8.

3.5. Thermal Expansion in Melt and Glassy State. On the basis of the simulated film density, we have calculated the non-normalized slopes $-(d\rho/dT)$ (Table 1) and the thermal expansion coefficients

$$\alpha = -\frac{1}{\rho}\left(\frac{d\rho}{dT}\right) \tag{6}$$

(Table 2) for films of different thicknesses and for different layers within the film; here ρ is the density of a whole film or corresponding layer. Note that the thermal expansion coefficients depend on the chosen temperature or density while the slopes are assumed piecewise constant for glass and melt. Obviously, the simulated slopes are higher for the melt states as compared to the glassy states (Table 1).

We found that for all simulated films the thermal expansion coefficients in the melt and in the glassy state practically do not show a trend with film thickness. Therefore, in Table 2, we present the values for the expansion coefficients averaged over all film thicknesses.

The bulk thermal expansion coefficients in Table 2 are taken from the PVT measurements for atactic PS with $M_w = 9 \times 10^3$ at atmospheric pressure[53] and from earlier simulations by one of us.[62]

We can compare our results on α with some literature data. On the basis of the data from ref 15, Forrest et al.[2] observed that the thermal expansivity of PS in the glassy state is indeed the same for all film thicknesses while for the liquid (melt) state the thermal expansivity decreases with decreasing film thickness. Our simulated average value of the thermal expansivity for a PS film in the melt is smaller than the corresponding bulk value from experiment and is within error bars comparable with the bulk value from simulations (see Table 2). The expansion coefficients for the simulated films are also comparable with the experimental values for PS films of ~9 nm, $\alpha_{melt} = 5.1 \times 10^{-4}$ K^{-1} [15] and of ~300 nm, $\alpha_{melt} = 5.9 \times 10^{-4}$ K^{-1}.[62]

3.6. Thickness Dependence of T_g. Figure 8a depicts the thickness dependence of the glass-transition temperature for the middle layer for different strengths of attraction to the substrate, as derived from the simulated average density. The glass-transition temperature in this layer practically does not depend on the thickness of the total film. It also depends only weakly on the strength of attraction. Its average value (for different films and different degrees of attraction)

$$T_g^{md} = 407 \pm 8 \text{ K} \tag{7}$$

is shown in Figure 8a by the dashed line. This temperature can serve as an indication of the glass-transition temperature in bulk aPS. Figure 8b shows the thickness dependence of T_g for the whole film using the simulated average density. In this case, some decrease of T_g with decreasing film thickness is observed, but only for very thin films, $H_f \leq 2$ nm. We note that this is in the range of the average radius of gyration (~2.0 nm), at least qualitatively in line with the observation in ref 45 that T_g should change at film thickness of the order $4R_g$.

We fitted the simulation data in Figure 8b by the empirical formula[4]

$$T_g(H_f) = T_g^{bulk}\left(1 - \left(\frac{A}{H_f}\right)^{\delta}\right) \tag{8}$$

where T_g^{bulk} is taken equal to T_g in the middle layer and H_f is the film thickness. For all data points the fit result A = 0.26 nm for the characteristic length is quite different from the value obtained by Keddie from ellipsometry experiments ($A = 3.2 \pm 0.6$ nm) but is rather close to that from dielectric studies by Fukao ($A = 0.39 \pm 0.10$ nm); the fitted exponent $\delta = 1.5$ is in between compared to those studies ($\delta = 1.8 \pm 0.2$ and $\delta = 0.96 \pm 0.08$, respectively).[3,21] The fit results A = 0.06 nm and $\delta = 0.9 \pm 0.3$ for the wetting (ε = 3.0 kcal/mol) substrate will be used for the further analysis in the Discussion section. Lattice MC simulations results for a model PS give A = 6.2 nm and δ = 1.71.[59]

While the glass-transition temperature of the middle layer only weakly depends on the strength of attraction to the substrate, T_g for the whole film fluctuates considerably with ε; however, no regular trend with the strength of attraction is observed. Obviously, the overall decrease of the glass-transition temperature with the film thickness for the whole film cannot be explained by the thickness dependence of the T_g values of the middle layer. Therefore, we have tried to study the thickness dependences of the T_g values in the substrate and surface layers.

For the majority of the simulated films the T_g values of the substrate layer increase above the bulk value (by ~20−50 K, depending on the strength of attraction to the substrate)

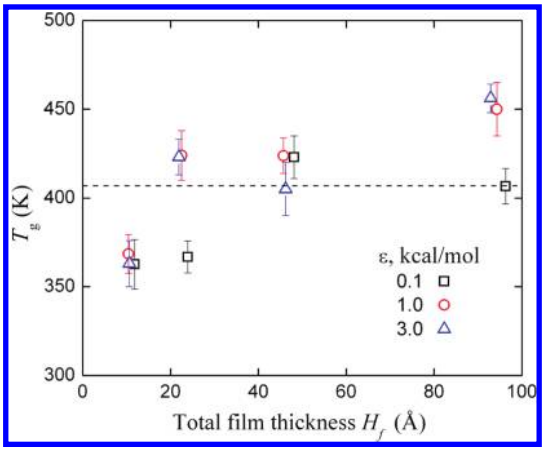

Figure 9. Thickness dependence of the T_g values for the substrate layer in aPS films with different strengths of attraction to the substrate.

(Figure 9). For the thicker ($H_f \sim 10$ nm) simulated film with a strong (ε = 1.0−3.0 kcal/mol) adsorption to the substrate the largest increase is observed, about 50 K.

Some saturation of this increase can be anticipated for thicker films, and the saturated value for T_g of the substrate layer is much larger than the value for T_g in bulk. The increase in substrate T_g is much smaller for thinner films. For a very thin film of ∼1.5 nm the substrate T_g even decreases by about 35 K compared to the bulk value.

In Figure 10, the results for the temperature dependence of the surface-layer density (a) and thickness (b) are shown, for 16-chain films with different strengths of attraction to the substrate. Both the density and the thickness remain almost constant with decreasing temperature; therefore, we were not able to identify a glass transition in this layer. We can only speculate that either the surface T_g is below the simulated temperature window or the fluctuations in the results are so big that the surface T_g cannot be defined with reasonable precision.

In summary, some decrease of T_g with total film thickness has been observed both for the average film and for the substrate layer, in particular for the thinnest films. No such decrease is seen in the middle layer, and no glass transition is seen at all in the surface layer. Qualitatively, these results hold both for weak and strong attraction, but systematic quantitative trends are not clear and error bars are rather large.

4. DISCUSSION

In many experiments and in the present simulations the glass transition both for the bulk and for a film is determined from the density by fitting two linear regions of data, at high and low temperatures, by straight lines:

$$\rho = \rho^0 + \left(\frac{d\rho}{dT}\right) T \tag{9}$$

and finding their intersection point. In this equation ρ^0 is the extrapolated density at $T = 0$. Solving the equations for the melt and glass regions, we produce the following expression for the glass-transition temperature:

$$T_g = -\frac{\rho_g^0 - \rho_m^0}{\left(\frac{d\rho}{dT}\right)_g - \left(\frac{d\rho}{dT}\right)_m} \tag{10}$$

Here we have m = melt and g = glass. The same expression can be obtained both for the bulk (notation T_g, ρ) and for a film (notation $\overline{T}_g$,). Combining these two expressions, we get an exact relation between the glass-transition temperature T_g for the bulk and $\overline{T}_g$ for a (density-averaged) thin film:

$$\frac{\overline{T}_g}{T_g} = \frac{1 + \dfrac{\delta\rho_g^0 - \delta\rho_m^0}{\rho_g^0 - \rho_m^0}}{1 + \dfrac{\dfrac{d}{dT}\delta\rho_g - \dfrac{d}{dT}\delta\rho_m}{\dfrac{d\rho_g}{dT} - \dfrac{d\rho_m}{dT}}} \tag{11}$$

Here $\delta\rho \equiv \overline{\rho} - \rho$ is the change in average density due to the confinement. From eq 11 it is clear that the confinement may have an effect on T_g, in particular through the effect on density via the presence of a free or attracting surface. That the confinement and attracting surface have an effect on density is evident from Figure 11: with decreasing film thickness the average density decreases or increases for weak or strong substrate attraction, respectively, as might be expected. However, the resulting effect on T_g is much more subtle for two reasons. First, there are effects both in the numerator and denominator of eq 11 which may compete. Second, due to the influence of the substrate, the density itself changes through the film in such a way that the film becomes stratified, with different densities and glass transitions in different layers.

To incorporate the effect of stratification into eq 11, the total film, with thickness H (we henceforth drop the subscript f) and density $\overline{\rho}$, can be split up in layers with thicknesses h_{sb} (substrate), h_{md} (middle), and h_{sf} (surface) and corresponding densities:

$$\overline{\rho} = \frac{1}{H} \sum_{i=\mathrm{sb,md,sf}} h_i \rho_i \tag{12}$$

If we assume that ρ_{md} is equal to the bulk density, as discussed before, the excess density is

$$\delta\overline{\rho} \equiv \overline{\rho} - \rho = \frac{h_{sb}\delta\rho_{sb} + h_{sf}\delta\rho_{sf}}{H} \equiv \frac{\delta m}{H} \tag{13}$$

By writing the excess density as in eq 13, the dominant dependence on thickness H is factored out, and the excess mass per unit area δm has a clear physical meaning: it is the amount of mass per unit area that redistributes itself (compared to the bulk) under the influence of the wetting/nonwetting substrate and the free surface (see Figure 6). In general, δm will depend on temperature and film thickness. If δm is independent of T, we can further simplify eq 11 via

$$\delta\rho_g^0 - \delta\rho_m^0 = \delta m \left[\left(\frac{1}{H}\right)_g^0 - \left(\frac{1}{H}\right)_m^0\right] \tag{14}$$

$$\frac{d}{dT}\delta\rho_g - \frac{d}{dT}\delta\rho_m = \delta m \left[-\frac{1}{H_g^2}\frac{dH_g}{dT} + \frac{1}{H_m^2}\frac{dH_m}{dT}\right] \tag{15}$$

Note that in eq 14 we use that $1/H$ and not H is fitted linear in T. In eq 15, the left-hand has been fitted as a constant, so we can evaluate right-hand side at $\overline{T}_g$:

$$\frac{d}{dT}\delta\rho_g - \frac{d}{dT}\delta\rho_m = -\frac{\delta m}{H(\overline{T}_g)}[\overline{\alpha}_g(\overline{T}_g) - \overline{\alpha}_m(\overline{T}_g)] \tag{16}$$

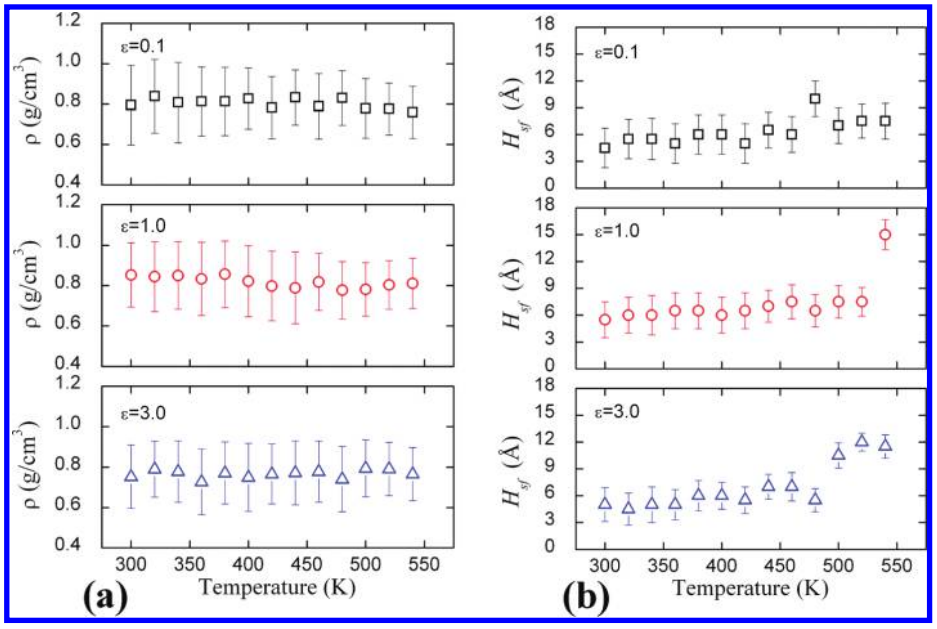

Figure 10. Temperature dependence of the density (a) and thickness (b) of the surface layer for the 16-chain films with different strengths of attraction to the substrate.

When we substitute eqs 14 and 16 into eq 11, we get as a result

$$\frac{\overline{T}_g}{T_g} = \frac{1 + C_1 \delta m / H(\overline{T}_g)}{1 + C_2 \delta m / H(\overline{T}_g)} \tag{17}$$

with

$$C_1 = \frac{[(1/H)_g^0 - (1/H)_m^0] H(\overline{T}_g)}{\rho_g^0 - \rho_m^0} \tag{18}$$

$$C_2 = \frac{1}{\rho(T_g)} \left[\frac{\overline{\alpha}_g(\overline{T}_g) - \overline{\alpha}_m(\overline{T}_g)}{\alpha_g(T_g) - \alpha_m(T_g)} \right] \tag{19}$$

While δm may still depend on film thickness, the coefficients C_1 and C_2 are true constants in the sense that they do not scale with H. Inserting order-of-magnitude estimates for all quantities at the right-hand sides of eqs 18 and eq 19, we see that both C_1 and C_2 will be of the order of 1 cm^3/g. So, whether T_g will actually increase or decrease with decreasing thickness H depends not only on the sign of δm (positive for a wetting surface, negative for a nonwetting surface; see Figure 11 and eq 13) but also on the sign of $\Delta C = C_1 - C_2$, i.e., on a subtle balance between the numerator and denominator of eq 17. The typical length scale over which T_g then varies with H is of the order $C_i \delta m$.

We still have to check whether the above analysis, with δm independent of T, applies to our simulated data. To that end we performed more detailed simulations of 32-chains films (N = 20 256 particles) for a strongly wetting substrate (ε = 3.0 kcal/mol), at four fixed different external pressures: 36, 37, 38, and 39 MPa. In this pressure range the density in the middle of the films and at T = 540 K centers around the experimental value (0.914 g/cm^3), with a maximum deviation of 1%. For these films the excess mass δm is presented in Figure 12 as a function of temperature. We observe that δm, first of all, is positive (in line with Figure 11 and eq 13) and, second, independent of T. By

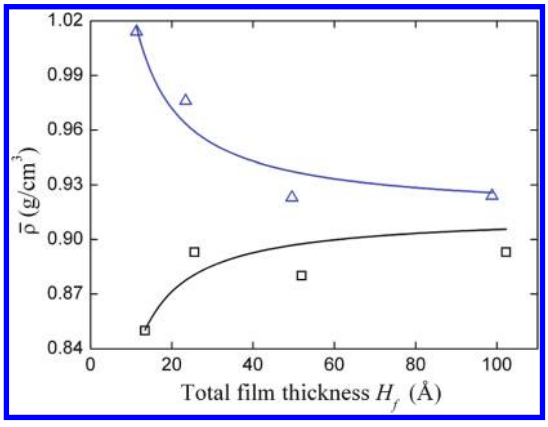

Figure 11. Average total film density versus total film thickness at T = 540 K for weak (ε = 0.1 kcal/mol, squares) and strong (ε = 3.0 kcal/mol, triangles) attraction to the substrate. The lines are fits to eq 13, with ρ fixed to the experimental value of 0.914 g/cm^3 in the middle of the film and δm as a free fitting parameter ($\delta m = -0.9 \times 10^{-8}$ g/cm^2 for ε = 0.1 kcal/mol and $\delta m = 1.2 \times 10^{-8}$ g/cm^2 for ε = 3.0 kcal/mol).

averaging δm over these four pressures and temperatures, we find $\delta m = (1.20 \pm 0.02) \times 10^{-8}$ g/cm^2.

That, in turn, gives $\delta N \sim 300$ particles that redistribute themselves between substrate and surface layers compared to a homogeneous film. On the basis of this, we calculate a characteristic length scale of the order of 0.1 nm, consistent with the fit value of A = 0.06 nm in Figure 8b and eq 8. Calculating C_1 and C_2 for these 32-chain strongly adsorbed films, we find that within relevant digits the coefficients are equal: $C_1 = C_2 = 1.1 \pm 0.2$ cm^3/g. Hence, any difference in C_1 and C_2, which will determine deviation of $\overline{T}_g$ from T_g, is in this case within the numerical error. So, given the subtle balance between the numerator and denominator in eq 17, our numerical data are too inaccurate to predict that T_g actually decreases for film thicknesses below 2 nm, as suggested by Figure 8b. We note that our observations are

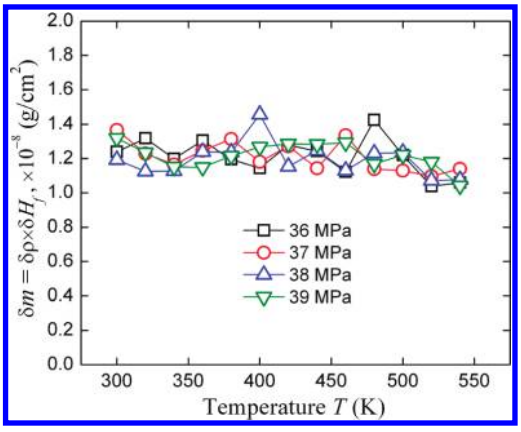

Figure 12. Excess mass δm as a function of temperature for films of 32 chains (strong wetting, ε = 3.0 kcal/mol), simulated at different external pressures.

nicely in line with a very recent experimental study by Tress et al.[63] on nanometric PS films, which shows by a range of techniques that T_g for films above 5 nm remains within a margin of ±3 K around the bulk value.

5. CONCLUSIONS

In the present study we have performed molecular dynamics simulations in order to investigate the possible influence of confinement on glass transition temperature T_g for supported atactic polystyrene films of different thickness H_f, from extremely thin (H_f = 1 nm) up to a thickness (10 nm) in the range where confinement effects have been reported experimentally.

We found some small orientation of both main-chain monomers and phenyl groups at the film surface and close to the substrate. This orientation disappears toward the middle of the film. Density profiles show that apart from this anisotropy the films are also heterogeneous in density, with a clearly stratified structure. On the basis of the analysis of the density profiles, we have defined three different layers (substrate, middle, and surface) for each film. The T_g value for the whole film as well as separate T_g values for the different layers have been extracted from the temperature dependence of the density or corresponding thickness. For the whole film the T_g value shows almost no thickness dependence for films down to 2 nm thickness, where the middle layer is completely absent; this is in line with very recent experimental data.[63] Some decrease of the T_g values is observed for thinner films, but statistical errors of these results are rather high. The T_g for the middle layer does not depend on the total film thickness either, and its density is close to the bulk density. For the substrate layer an increase in T_g up to 50 K is measured depending on the strength of attraction to the substrate. The surface layer remains liquid-like in the whole temperature range (300−540 K).

Dynamic heterogeneity of supported thin polymer films was shown by Baljon et al. by means of molecular dynamics simulations of bead−spring chains.[64] It was already observed that on average immobile clusters more frequently occur near a strongly attracting surface. At temperatures around the glass-transition temperature the clusters of immobile beads start to percolate in the direction perpendicular to the substrate. However, no quantitative study was made yet of the average density or the precise value of T_g. In this respect our approach is more detailed since in the present article we have determined an effective T_g by measuring the average film density. Moreover, we have shown that the density in such films is stratified, with different glass-transition temperatures in different film layers. It should be also noticed that in the present study we do not calculate the segmental mobility in these three film layers. Instead, only the statistical equilibrium properties of thin PS films have been investigated. From the viewpoint of polymer segmental dynamics these layers are different, and the free interface and the substrate layer definitely might compete when calculating the average glass transition temperature. The goal of the present study was to investigate another competition between these three layers, mainly in terms of the redistribution of mass between substrate, surface, and the middle of films. As we show, such a mass redistribution influences the average T_g dependence on the film thickness but in very subtle way.

In view of the reported stratification of the internal film structure, a glass-transition temperature T_g that is based on the temperature dependence of the average density has actually limited physical meaning for what happens near the substrate, a fact often ignored in experiment. Through a more detailed analysis of the effect of stratification we have been able to express the change in this effective T_g in terms of the film thickness and average density and in the extent of mass redistribution with respect to the homogeneous bulk polymer. The expression shows that an increase or decrease of the density-based effective T_g with decreasing film thickness depends on a subtle balance of detailed effects and has no straightforward relation with average density or with strength of substrate attraction. Our numerical data are consistent with the derived expression but too inaccurate to make predictions on the change of the effective glass-transition temperature.

■ ACKNOWLEDGMENT

This study is a part of the research program of the Dutch Polymer Institute, project #654. This work was also sponsored by the Stichting Nationale Computerfaciliteiten (National Computing Facilities Foundation, NCF) for the use of supercomputer facilities, with financial support from the Nederlandse Organisatie voor Wetenschappelijk Onderzoek (Netherlands Organization for Scientific Research, NWO). The stimulating discussions with M. Wübbenhorst, A. Serghei, and G. B. McKenna are gratefully acknowledged.

■ REFERENCES

(1) Roth, C. B.; Dutcher, J. R. *J. Electroanal. Chem.* **2005**, *584*, 13–22.
(2) Forrest, J. A.; Dalnoki-Veress, K. *Adv. Colloid Interface Sci.* **2001**, *94*, 167–196.
(3) Keddie, J. L.; Jones, R. A. L.; Cory, R. A. *Europhys. Lett.* **1994**, *27*, 59–64.
(4) Keddie, J. L.; Jones, R. A. L. *Faraday Discuss.* **1994**, *98*, 219–230.
(5) Kawana, S.; Jones, R. A. L. *Phys. Rev. E* **2001**, *63*, 021501.
(6) Seemann, R.; Jacobs, K.; Landfester, K.; Herminghaus, S. *J. Polym. Sci., Part B: Polym. Phys.* **2006**, *44*, 2968–2979.
(7) Fakhraai, Z.; Forrest, J. A. *Phys. Rev. Lett.* **2005**, *95*, 025701.
(8) Fakhraai, Z.; Sharp, J. S.; Forrest, J. A. *J. Polym. Sci., Part B: Polym. Phys.* **2004**, *42*, 4503–4507.
(9) Dalnoki-Veress, K.; Forrest, J. A.; Murray, C.; Gigault, C.; Dutcher, J. R. *Phys. Rev. E* **2001**, *63*, 031801.
(10) Forrest, J. A.; Dalnoki-Veress, K.; Dutcher, J. R. *Phys. Rev. E* **1997**, *56*, 5705–5716.

(11) Forrest, J. A.; Dalnoki-Veress, K.; Dutcher, J. R. *Phys. Rev. E* **1998**, *58*, 6109–6114.
(12) Forrest, J. A.; Dalnoki-Veress, K.; Stevens, J. R.; Dutcher, J. R. *Phys. Rev. Lett.* **1996**, *77*, 2002–2005.
(13) Tsui, O. K. C.; Rusell, T. P.; Hawker, C. J. *Macromolecules* **2001**, *34*, 5535–5539.
(14) Ahn, S. I.; Kim, J.-H.; Kim, J. H.; Jung, J. C.; Chang, T.; Ree, M.; Zin, W.-C. *Langmuir* **2009**, *25*, 5667–5673.
(15) Wallace, W. E.; van Zanten, J. H.; Wu, W. L. *Phys. Rev. E* **1995**, *52*, 3329–3332.
(16) Kanaya, T.; Miyazaki, T.; Inoue, R.; Nishida, K. *Phys. Status Solidi* **2005**, *242*, 595–606.
(17) Inoue, R.; Kanaya, T.; Miyazaki, T.; Nishida, K.; Tsukushi, I.; Shibata, K. *Mater. Sci. Eng., A* **2006**, *442*, 367–370.
(18) DeMaggio, G. B.; Frieze, W. E.; Gidley, D. W.; Ming, Z.; Hristov, H. A.; Yee, A. F. *Phys. Rev. Lett.* **1997**, *78*, 1524–1527.
(19) Wallace, W. E.; Beck Tan, N. C.; Wu, W. L.; Satija, S. *J. Chem. Phys.* **1998**, *108*, 3798–3804.
(20) Kanaya, T.; Miyazaki, T.; Watanabe, H.; Nishida, K.; Yamano, H.; Tasaki, S.; Bucknall, D. B. *Polymer* **2003**, *44*, 3769–3773.
(21) Fukao, K.; Miyamoto, Y. *Phys. Rev. E* **2000**, *61*, 1743–1754.
(22) Priestley, D. R.; Broadbelt, L. J.; Torkelson, J. M.; Fukao, K. *Phys. Rev. E* **2007**, *75*, 061806.
(23) Svanberg, C. *Macromolecules* **2007**, *40*, 312–315.
(24) Serghei, A.; Huth, H.; Schick, C.; Kremer, F. *Macromolecules* **2008**, *41*, 3636–3639.
(25) Lupaşcu, V.; Huth, H.; Schick, C.; Wübbenhorst, M. *Thermochim. Acta* **2005**, *432*, 222–228.
(26) Lupaşcu, V.; Picken, S. J.; Wübbenhorst, M. *J. Non-Cryst. Solids* **2006**, *352*, 5594–5600.
(27) Efremov, M. Y.; Olson, E. A.; Zhang, M.; Zhang, Z.; Allen, L. H. *Phys. Rev. Lett.* **2003**, *91*, 085703.
(28) Efremov, M. Y.; Olson, E. A.; Zhang, M.; Zhang, Z.; Allen, L. H. *Macromolecules* **2004**, *37*, 4607–4616.
(29) Fryer, D. S.; Nealey, P. F.; de Pablo, J. J. *Macromolecules* **2000**, *33*, 6439–6447.
(30) Torres, J. A.; Nealey, P. F.; de Pablo, J. J. *Phys. Rev. Lett.* **2000**, *85*, 3221–3224.
(31) Böhme, T. R.; de Pablo, J. J. *J. Chem. Phys.* **2002**, *116*, 9939–9951.
(32) Varnik, F.; Baschnagel, J.; Binder, K. *Eur. Phys. J. E* **2002**, *8*, 175–192.
(33) Baschnagel, J.; Varnik, F. *J. Phys.: Condens. Matter* **2005**, *17*, R851–R953.
(34) Peter, S.; Meyer, H.; Baschnagel, J. *Polym. Sci., Part B: Polym. Phys.* **2006**, *44*, 2951–2967.
(35) Peter, S.; Meyer, H.; Baschnagel, J.; Seemann, R. *J. Phys.: Condens. Matter* **2007**, *19*, 205119.
(36) Götze, W.; Sjögren, L. *Rep. Prog. Phys.* **1992**, *55*, 241–376.
(37) Mansfield, K. F.; Theodorou, D. N. *Macromolecules* **1991**, *24*, 6283–6294.
(38) Zeghal, M.; Deloche, B.; Auroy, P. *Macromolecules* **1999**, *32*, 4947–4955.
(39) Rivilion, S.; Auroy, P.; Delonche, B. *Phys. Rev. Lett.* **2000**, *84*, 499–502.
(40) Maksimov, A. V.; Pavlov, G. M. *Polym. Sci., Ser. A* **2007**, *49*, 828–836.
(41) Grishchenko, A. E.; Mikhaĭlova, N. A.; Kononov, A. I.; Rudakova, T. V.; Mel'nikov, A. B. *J. Opt. Technol.* **2009**, *76*, 167–169.
(42) Kolinski, A.; Smolnick, J.; Yaris, R. *Macromolecules* **1986**, *19*, 2550–2560.
(43) Bliznyuk, V. N.; Assender, H. E.; Briggs, G. A. D. *Macromolecules* **2002**, *35*, 6613–6622.
(44) Ellison, C. J.; Torkelson, J. M. *Nature Mater.* **2003**, *2*, 695–700.
(45) Mukhopadhyay, M. K.; Jiao, X.; Lurio, L. B.; Jiang, Z.; Stark, J.; Sprung, M.; Narayanan, S.; Sandy, A. R.; Sinha, S. K. *Phys. Rev. Lett.* **2008**, *101*, 115501.
(46) Baljon, A. R. C.; Williams, S.; Balabaev, F.; Paans, F.; Hudzinskyy, D.; Lyulin, A. V. *J. Polym. Sci., Part B: Polym. Phys.* **2010**, *48*, 1160–1167.
(47) Mondello, M.; Yang, H. J.; Furuya, H.; Roe, R. J. *Macromolecules* **1994**, *27*, 3566–3574.
(48) Vorselaars, B.; Lyulin, A. V.; Michels, M. A. J. *Macromolecules* **2007**, *40*, 6001–6011.
(49) Müller, M.; MacDowell, L. G. *J. Chem. Phys.* **2002**, *118*, 2929–2940.
(50) William, A. S. In *The Interaction of Gases with Solid Surfaces*; Pergamon: London, 1974; p 349.
(51) Allen, M. P.; Tildesley, D. J. In *Computer Simulation of Liquids*; Clarendon Press: Oxford, 1987; p 385.
(52) Lemak, A. S.; Balabaev, N. K. *J. Comput. Chem.* **1996**, *17*, 1685–1695.
(53) Zoller, P.; Walsh, D. J. In *Standard Pressure-Volume-Temperature Data for Polymers*; Technomic: Lancaster, 1995; p 412.
(54) Lyulin, A. V.; Michels, M. A. J. *Phys. Rev. Lett.* **2007**, *99*, 085504.
(55) Yoon, D. Y.; Sundararajan, P. R.; Flory, P. J. *Macromolecules* **1975**, *8*, 776–783.
(56) Vorselaars, B.; Lyulin, A. V.; Michels, M. A. J. *Macromolecules* **2009**, *42*, 5829–5842.
(57) Wittmer, J. P.; Meyer, H.; Baschnagel, J.; Johner, A.; Obukhov, S.; Mattioni, L.; Müller, M.; Semenov, A. N. *Phys. Rev. Lett.* **2004**, *93*, 147801.
(58) Mulder, T.; Harmandaris, V. A.; Lyulin, A. L.; van der Vergt, N. F. A.; Kremer, K.; Michels, M. A. J. *Macromolecules* **2009**, *42*, 384–391.
(59) Wittmer, J. P.; Beckrich, P.; Meyer, H.; Cavallo, A.; Johner, A.; Baschnagel, J. *Phys. Rev. E* **2007**, *76*, 011803.
(60) Jain, T. S.; de Pablo, J. J. *Macromolecules* **2002**, *35*, 2167–2176.
(61) Baljon, A. R. C.; van Weert, M. H. M.; DeGraaff, R. B.; Khare, R. *Macromolecules* **2005**, *38*, 2391–2399.
(62) Lyulin, A. V.; Michels, M. A. J. *Macromolecules* **2002**, *35*, 1463–1472.
(63) Tress, M.; Erber, M.; Mapesa, E. U.; Huth, H.; Müller, J.; Serghei, A.; Schick, C.; Eichhorn, K.-J.; Voit, B.; Kremer, F. *Macromolecules* **2010**.
(64) Baljon, A. R. C.; Billen, J.; Khare, R. *Phys. Rev. Lett.* **2004**, *93*, 255701.

NOTE ADDED AFTER ASAP PUBLICATION

This article posted ASAP on March 9, 2011. Equations 5 and 11 have been revised. The correct version posted on March 11, 2011.